PCCP

PAPER

View Article Online
View Journal | View Issue

Cite this: *Phys. Chem. Chem. Phys.*, 2022, **24**, 14886

Extensive characterization of choline chloride and its solid–liquid equilibrium with water†

Ana I. M. C. Lobo Ferreira, [a] Sérgio M. Vilas-Boas, [bc] Rodrigo M. A. Silva, [a] Mónia A. R. Martins, [c] Dinis. O. Abranches, [c] Paula C. R. Soares-Santos, [c] Filipe A. Almeida Paz, [c] Olga Ferreira, [b] Simão P. Pinho, *[b] Luís M. N. B. F. Santos *[a] and João A. P. Coutinho [c]

The importance of choline chloride (ChCl) is recognized due to its widespread use in the formulation of deep eutectic solvents. The controlled addition of water in deep eutectic solvents has been proposed to overcome some of the major drawbacks of these solvents, namely their high hygroscopicities and viscosities. Recently, aqueous solutions of ChCl at specific mole ratios have been presented as a novel, low viscous deep eutectic solvent. Nevertheless, these proposals are suggested without any information about the solid–liquid phase diagram of this system or the deviations from the thermodynamic ideality of its precursors. This work contributes significantly to this matter as the phase behavior of pure ChCl and (ChCl + H_2O) binary mixtures was investigated by calorimetric and analytical techniques. The thermal behavior and stability of ChCl were studied by polarized light optical microscopy and differential scanning calorimetry, confirming the existence of a solid–solid transition at 352.2 ± 0.6 K. Additionally, heat capacity measurements of pure ChCl (covering both ChCl solid phases) and aqueous solutions of ChCl ($x_{ChCl} < 0.4$) were performed using a heat-flow differential scanning microcalorimeter or a high-precision heat capacity drop calorimeter, allowing the estimation of a heat capacity change of (ChCl) ≈ 39.3 ± 10 J K^{-1} mol^{-1}, between the hypothetical liquid and the observed crystalline phase at 298.15 K. The solid–liquid phase diagram of the ChCl + water mixture was investigated in the whole concentration range by differential scanning calorimetry and the analytical shake-flask method. The phase diagram obtained for the mixture shows an eutectic temperature of 204 K, at a mole fraction of choline chloride close to x_{ChCl} = 0.2, and a shift of the solid–solid transition of ChCl–water mixtures of 10 K below the value observed for pure choline chloride, suggesting the appearance of a new crystalline structure of ChCl in the presence of water, as confirmed by X-ray diffraction. The liquid phase presents significant negative deviations to ideality for water while COSMO-RS predicts a near ideal behaviour for ChCl.

Received 23rd January 2022,
Accepted 20th April 2022

DOI: 10.1039/d2cp00377e

rsc.li/pccp

Introduction

Choline chloride (ChCl) is an organic salt used as an *x* additive in animal feed.[1] The interest of the research community in this compound has increased significantly in the last two decades, mainly due to its use in the preparation of deep eutectic solvents (DESs). A search conducted on the Web of Science core collection on January 9th, 2022, for the topic "choline chloride", showed 5300 scientific articles, whereas the results were reduced to just 815 papers by limiting the search up to 2003, when Abbott and co-authors suggested using ChCl-based eutectic mixtures as novel solvents.[2] Since then, several ChCl-based DESs have been proposed[3–8] for an extensive range of applications.[9–14] Apart from the hydrogen bond acceptor nature of ChCl,[15] this ionic compound presents desirable properties to be explored in the formulation of DESs, such as low toxicity, biodegradability, low cost and large scale availability.[16–18]

Although DESs have been proposed as promising solvents to be applied in several areas, including metal processing[9] and the extraction of a broad set of substances,[19] its use at an industrial scale often encounters some practical obstacles, mainly due to their high hygroscopicities and viscosities.[16,20] An alternative recently proposed to overcome this issue is the controlled addition of water to these mixtures,[7] which generally leads to

[a] *CIQUP, Institute of Molecular Sciences (IMS) – Departamento de Química e Bioquímica, Faculdade de Ciências da Universidade do Porto, Rua Campo Alegre, 4169-007 Porto, Portugal. E-mail: lbsantos@fc.up.pt; Fax: +351 273 313 051; Tel: +351 273 303 086*

[b] *Centro de Investigação de Montanha (CIMO), Instituto Politécnico de Bragança, Campus de Santa Apolónia, 5300-253 Bragança, Portugal. E-mail: spinho@ipb.pt*

[c] *CICECO – Aveiro Institute of Materials, Department of Chemistry, University of Aveiro, 3810-193 Aveiro, Portugal*

† Electronic supplementary information (ESI) available. See DOI: https://doi.org/10.1039/d2cp00377e

a decrease of their viscosity,[7] but it might also modify other relevant physicochemical properties, such as ionic conductivity and density.[21] In fact, the use of water in the formulation of DESs is economically and environmentally desirable since water is abundant, cheap, non-flammable, and nontoxic. However, its presence in the mixture should be carefully investigated since water might bring structural changes in the DES intermolecular network due to its highly polar nature.[21]

The large majority of studies investigating the role of water in DESs are related to mixtures of choline chloride with well-known hydrogen bond donors, such as lactic acid,[7,22] urea,[23–27] glycols,[7,26–31] and sugars.[7] Recently, it was suggested that aqueous solutions of choline chloride, with a certain mole ratio, were also deep eutectic solvents.[32–34] Triolo and co-authors[33] proposed "the first water-in-salt (WiS) natural deep eutectic solvent (NADES), hereinafter indicated as aquoline, a mixture of choline chloride (ChCl) and water with a molar ratio of 1 : 3.33″ without considering adequately the solid–liquid phase diagram (SLPD) of the choline chloride + water mixture. Although the authors used the available solid–liquid equilibrium (SLE) information,[32,35] those data covered only part of the SLPD of this important mixture. Moreover, as we discussed elsewhere,[18] to name a certain proportion (1 : 3.33) of two compounds as a new substance (aquoline[33]) is not adequate. Additionally, the attraction to have fixed proportions to define eutectic compositions is unwise and sometimes drives to intriguing statements. Zhang *et al.*,[32] instead of presenting the mole fraction composition of the eutectic point found in their study, preferred to write, "We found that the aqueous dilution of ChCl/2H_2O with a ChCl/2H_2O content of *ca.* 80 wt% was an eutectic".

In this context, a detailed characterization of the thermal behavior of pure choline chloride and a full description of the solid–liquid phase diagram of the choline chloride + water mixture is proposed here. First, the thermal behavior and stability of pure ChCl were investigated by differential scanning calorimetry and polarized light optical microscopy. Additionally, the heat capacity measurements of pure ChCl were conducted using a high-precision heat capacity drop calorimeter at 298.15 K and then in the temperature range from 283 to 419 K covering both ChCl solid phases using a heat-flow differential scanning microcalorimeter. Lastly, the heat capacity measurements were extended to aqueous solutions of ChCl (mole fractions ChCl < 0.4) at 298.15 K, enabling the estimation of the hypothetical heat capacity of ChCl in the liquid phase at this temperature. Then, to characterize the phase diagram of the choline chloride + water mixture, measurements were carried out for mixtures in the entire composition range, by differential scanning calorimetry and the analytical shake flask method. The results are discussed in terms of the non-ideality of the liquid phase.

Experimental

Chemicals

Choline chloride (≥99% Sigma, CAS 67-48-1) was purified under vacuum (<10 Pa) at T = 353 K for 72 h and kept under vacuum before use. The water content of the purified sample (<110 ppm) was checked using a Karl-Fischer titrator (Metrohm, model 831 KF Coulometer) equipped with an 860 KF Thermoprep system. All samples were prepared and manipulated in a glove box under dry nitrogen and maintained in hermetic flasks under inert atmosphere. Double distilled water, passed through a reverse osmosis system and further treated with a MilliQ plus 185 water purification apparatus, was used in the preparation of all binary solutions. Purity analyses of water revealed a resistivity value of 18.2 MΩ cm and a TOC (total organic carbon content) of lower than 5 μg dm^{-3}.

Microscopy studies of choline chloride

The solid–solid transition of choline chloride was studied by polarized light optical microscopy using an Olympus microscope model BX51. The sample images were acquired using an optical Olympus C5060 digital compact camera. The samples, finely powdered, were prepared in a glove box under a dry nitrogen atmosphere and the experiments were also performed under a dry nitrogen atmosphere. The temperature was accurately controlled using a Linkam TMHS600 heating stage (±0.1 °C) controlled by a TP94 unit.

Powder X-ray diffraction of choline chloride

The dry and air equilibrated (for 24 h) samples of choline chloride were ground and homogenized in an agate mortar and analyzed by *in situ* powder X-ray diffraction (air room conditions 296.2 K and relative humidity < 37%) for crystalline phase characterization. Powder X-ray diffraction (PXRD) data were collected using a Empyrean PANalytical diffractometer (Almelo, Netherlands) equipped with an Anton Paar TTK chamber and the TCU temperature control unit, in the Bragg–Brentano *para*-focusing optics configuration with Cu K$\alpha_{1,2}$ X-radiation (λ_1 = 1.540598 Å; λ_2 = 1.544426 Å), equipped with a Ni filter (0.020 mm thickness) and a linear PIXcel 1D detector (active length 3.3473°), and a flat-plate spinner sample holder in the Bragg–Brentano *para*-focusing optics configuration (45 kV, 40 mA). The intensity data were collected using the continuous counting method (step 0.0131°) in the *ca.* $10^\circ \leq 2\theta \leq 60^\circ$ range, at 298, 348 and 358 K. The difractograms of the dry samples are in good agreement with the structures of the α and β phases of choline chloride previously reported. The wet diffractograms at 348 and 358 K are similar and the indexation of the 358 K diffractogram was performed.

The collected powder X-ray diffraction pattern was indexed using the LSI-Index algorithm implemented in TOPAS-Academic V5.[36,37] The crystal structure was determined in TOPAS-Academic V5[36] by using a simulated annealing approach. Rietveld structural refinements[38] were performed in the same programme using a Chebychev polynomial throughout the entire angular range to model the background contribution. The peak shapes of the powder pattern were described using the fundamental parameter approach.[39] In the ESI† (Section S1), all the details pertaining to the powder X-ray data collection, crystal data and structure refinement details of the wet ChCl structure at 358 K are gathered.

Solid-state NMR studies

$^{13}C\{^{1}H\}$ cross-polarization magic-angle spinning (CP MAS) NMR spectra were acquired using a Bruker Avance III 400 spectrometer operating at a magnetic field of 9.4 T with a ^{13}C Larmor frequency of 100.6 MHz.

The spectra of pure choline chloride, packed into a ZrO_2 rotor with a Vespel cap, were recorded at room temperature and at 358 K using a triple-resonance 4 mm probe and a BVT3000 unit for the temperature control. The $^{13}C\{^{1}H\}$ CP MAS spectra were acquired with a ^{1}H 90° pulse set to 3.0 μs, 3 ms contact time using a 70–100% RAMP shape at the ^{1}H channel and using a 55 kHz square shape pulse on the ^{13}C channel, 5 s recycle delays. During the acquisition, a SPINAL-64 decoupling scheme was employed using a pulse length of 5.75 μs at an RF field strength of 83 kHz. Chemical shifts are quoted in ppm from α-glycine (secondary reference, C═O at 176.03 ppm).

Thermal behavior studies of pure choline chloride

The thermal behavior of choline chloride was measured using a power compensation differential scanning calorimeter DSC, PerkinElmer model Pyris Diamond DSC. The temperature and heat flux scales of the DSC were calibrated by measuring the temperature and the enthalpy of the fusion of reference materials,[40,41] namely, benzoic acid,[42] perylene,[41] 1,3,5-triphenylbenzene,[41] *o*-terphenyl,[41] anthracene,[41] naphthalene,[40] diphenyl ether,[40] 1,3-difluorobenzene,[40] 1-heptanol,[43] and 1-hexanol,[43] at a temperature scanning rate of 0.0833 K s^{-1}. All the experiments were performed under an inert atmosphere using a constant flow of N_2 (g) (50 mL min^{-1}) and hermetically sealed aluminium crucibles of 50 μL. The mass of the samples (about 5–20 mg) was measured using an ultra-microbalance Mettler Toledo model UMT2, with a readability of 0.1 μg and an experimental repeatability of 0.2 μg. The detailed experimental results and procedure, concerning the phase behavior of ChCl, are given in the ESI† (Section S2).

High precision heat capacity measurements

The heat capacities at T = 298.15 K of choline chloride were measured using a high-precision heat capacity drop calorimeter, already described in detail in the literature.[44–47] Details concerning the calibration and accuracy tests as well as the row experimental data are provided in the ESI† (Section S3). The stated accuracy of this methodology for the measurements of the heat capacities of liquids and solids at T = 298.15 K is better than 0.5%.

Temperature dependence of the heat capacity

The standard molar heat capacities (p = 10^5 Pa) of the α crystalline phase of the pure choline chloride were measured (more details in ESI,† Section S4) in the temperature range between 283 and 333 K with an uncertainty of 0.5%, *via* heat-flow differential scanning microcalorimetry (HC-DSC), using a SETARAM microDSC III. Furthermore, the heat capacity of the β crystalline phase was also measured, with an estimated uncertainty of 3%, in the temperature range between 363 and 419 K by power compensation differential scanning calorimetry (DSC), using a PerkinElmer PYRIS Diamond DSC. In the latter apparatus, highly pure (99.999%) gaseous nitrogen was used as protective gas (50 ml min^{-1}). Regarding the experimental procedure, in both cases, the isothermal step method was used, and the calibration was performed using highly pure synthetic sapphire (α-Al_2O_3, NBS SRM-720).[40,48] For the HC-DSC measurements, ΔT_{step} = 10 K, heating rate = 0.3 K min^{-1}, $t_{isothermal}$ = 2400 s and for the DSC measurements, ΔT_{step} = 5 K, heating rate = 5 K min^{-1}, $t_{isothermal}$ = 600 s conditions were applied. All samples were prepared in a glovebox under a dry nitrogen atmosphere.

The experimental solid–liquid equilibrium of ChCl + water mixtures

The SLE of the choline chloride + water mixtures was investigated using three different methodologies:

Procedure 1 – differential scanning calorimetry. The SLE data of the aqueous solutions of mole fractions of ChCl between 0.007 and 0.329 were investigated using a differential scanning calorimeter (NETZSCH, model 204 F1 Phoenix, combined with a closed-loop intracooler unit) using a nitrogen flowing system. The methodology employed here is based on the theory developed by Kousksou and co-authors,[49,50] in which the freezing points of ice in equilibrium with ethanol + water mixtures were determined from the consecutive heating–cooling DSC cycles with different heating rates. The authors found out that there is a linear relationship between the measured peak melting temperature of ice and the specific flow rate registered by the DSC at different heating rates, and then the equilibrium temperature can be calculated at a hypothetical heating rate of 0 K min^{-1}, corresponding to the corrected water freezing point in the mixture. Besides the well-description of the SLE of the aqueous solution of ethanol, this methodology has been successfully employed to describe the freezing points of ice in other binary aqueous solutions.[51–53]

Procedure 2 – differential scanning calorimetry. The SLE data of the aqueous solutions of mole fractions of ChCl between 0.100 and 0.901 were investigated using a differential scanning calorimeter (PerkinElmer model Pyris Diamond DSC) at a heating rate of 0.0833 K s^{-1} (5 K min^{-1}) and a constant flow of high purity (99.999%) gaseous nitrogen as the protective gas. A detailed description of the sample preparation and thermal procedures is presented in Sections S5 and S6 of the ESI.†

Procedure 3 – the shake-flask method. The solubility of the aqueous solutions of choline chloride with salt mole fractions within the range of 0.486–0.515 was carried out by the isothermal shake-flask method, which is described in detail in previous studies by our group.[35,54,55] A small excess amount of choline chloride was added in a sealed glass flask containing around 50 ml of water. The flask was placed in an isothermal bath equipped with an external temperature Pt100 sensor (±0.1 K). The mixture was agitated for at least 6 hours, followed by at least 12 hours of settling, which was found to be the minimum required conditions to reach the equilibrium. Then, at least three independent samples of around 3 cm^3 were removed from the mother solution using all-glass syringes coupled with nylon filters (0.45 μm pore size). Each sample was diluted in ultra-pure water

and analyzed by refractometry (Anton Paar, model Abbemat 500) with a reproducibility within $\pm 5.10^{-5}$. Each reported data point was calculated as the average value of at least six readings.

Results and discussion

The thermal behavior and stability of choline chloride

Fig. 1 depicts the solid–solid transition from phase α to phase β of an experiment performed at a scanning rate of 0.083 K s^{-1} (5 K min^{-1}), where the crystals of choline chloride were heated from 298 K to 353 K (an isothermal step of $t_{isothermal}$ = 200 s) followed by cooling at a same scanning rate until 298 K. The micrographs presented were taken at temperatures of 343 and 353 K in both the heating and the cooling cycles. It is possible to see, from pictures A, B and D, that phase α shows birefringence crystals and that phase β (picture C) does not show an observable birefringence.

The morphology change of the dry ChCl at relatively high temperatures and scanning rates was also evaluated in order to have an optical evaluation of the decomposition process. Fig. 2 presents optical images from T_i = 298 K to T_f = 673 K, at a scanning rate of 1.5 K s^{-1} (90 K min^{-1}). At T = 607 K, the yellow coloration indicates the beginning of the ChCl decomposition in excellent agreement with the DSC results (Section S2 of the ESI†). The crystalline type material of ChCl can be observed until T = 670 K; after this temperature, a full decomposition occurs, which is also in agreement with the observed DSC measurements performed at the same scanning rate.

In order to complement the study of the decomposition of ChCl by polarized light optical microscopy, the kinetics of decomposition was followed by DSC. The onset temperature of the decomposition process, T_{dec}, was evaluated at different scanning rates (5, 10, 20, 90 and 200 K min^{-1}). The detailed experimental data are available in the ESI† (Section S2). Fig. 3 depicts the fitting between the ln(scanning rate/(K min^{-1})) and $1/T$ (K^{-1}).

The linear dependency observed between ln(scanning rate /(K min^{-1})) and $1/T$ (K^{-1}) is a strong indication of a kinetic controlled decomposition process.

The solid–solid transition of choline chloride

In order to evaluate a possible effect of the thermal history in the solid–solid transition of choline chloride, the same sample and crucible were submitted to repeated temperature cycles by DSC, submitting the sample to a successive increase of the oven temperature (after the temperature of transition). Fig. 4 depicts the thermograms of successive heating and cooling at a scanning rate of 0.0833 K s^{-1} (5 K min^{-1}) from T_i = 298 K to T_f = 368 K in the first run; to T_f = 423 K in the second run; and in the last run the final temperature of the scanning run was

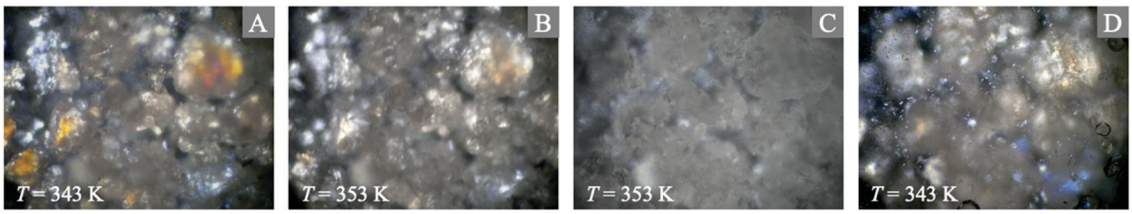

Fig. 1 Illustrative polarized light optical microscopy micrographs of the choline chloride solid–solid transition performed at a scanning rate of 0.083 K s^{-1}. Magnification 400×. (A) α phase at 343 K (heating cycle); (B) α phase at 353 K; (C) β phase at 353 K; (D) α phase at 343 K (cooling cycle).

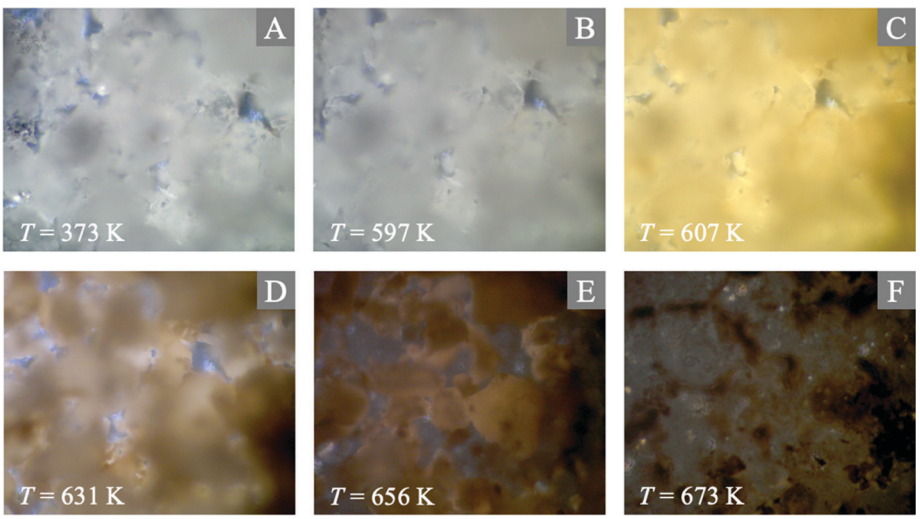

Fig. 2 Illustrative polarized light optical microscopy micrographs of pure choline chloride (scanning rate 90 K min^{-1}). Magnification 400×.

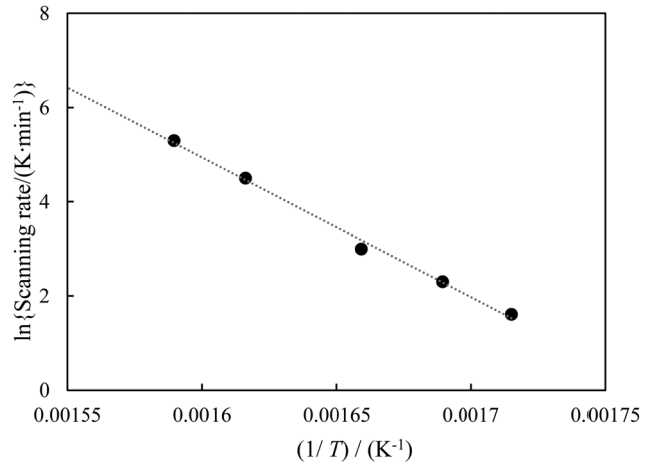

Fig. 3 Plot of ln(scanning rate/(K min^{-1})) as a function of the inverse of the onset temperature of decomposition, 1/T (K^{-1}): ln(scanning rate/(K min^{-1})) = $-29.7 \times 10^3/T$ (K^{-1}) + 52.4.

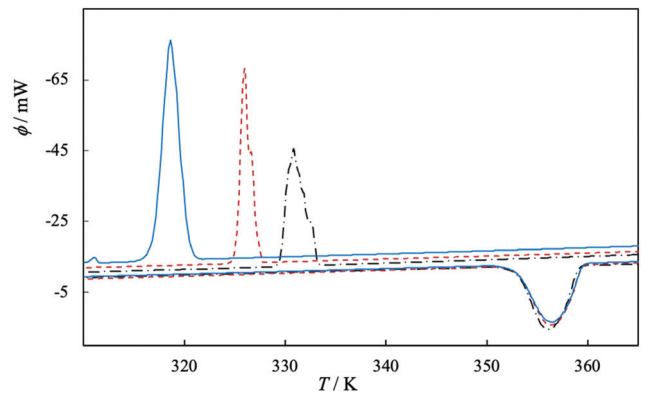

Fig. 4 DSC thermograms for choline chloride (7.4 mg) heat flow *versus* the temperature: scanning rate = 5 K min^{-1}: — 1st run, T_i = 298 K and T_f = 368 K; — 2nd run, T_i = 298 K and T_f = 423 K; and — 3rd run, T_i = 298 K and T_f = 513 K.

T_f = 513 K. No significant change on the shape and onset temperature was observed from α to β upon the heating process. The reverse solid–solid transition process (β to α, upon cooling) presents a small (20 to 30 K) undercooled temperature offset, which is dependent of the thermal history, temperature scanning rate, sample size, *etc.* (*e.g.* as depicted in Fig. 4). Overall, the observed solid–solid transition (α to β) is reversible and associated with higher enthalpic and entropic changes.

Table 1 summarizes the results obtained by DSC, concerning the (α to β) solid–solid transition at a standard pressure (p° = 0.1 MPa), namely: temperature T_{ss}, molar enthalpy $\Delta^{s\beta}_{s\alpha}H^\circ_m(T_{ss})$, and molar entropy $\Delta^{s\beta}_{s\alpha}S^\circ_m(T_{ss})$ of the (α to β) solid–solid transition. These results are in excellent agreement with the results by Petrouleas and Lemmon.[56] Moreover, the observed heat capacity change associated with the solid–solid transition $\Delta^{s\beta}_{s\alpha}C^\circ_{p,m} = 16 \pm 5$ J K^{-1} mol^{-1} (derived from the heat flow base line change at the (α to β) transition, following the methodology described by Serra *et al.*[57]), is remarkably high, in line with the high enthalpic and entropic changes associated with this phase.

Table 1 Solid–solid transition temperature, T_{ss}, standard (p° = 10^5 Pa) molar enthalpy, $\Delta^{s\beta}_{s\alpha}H^\circ_m(T_{ss})$, and entropy, $\Delta^{s\beta}_{s\alpha}S^\circ_m(T_{ss})$, of the solid–solid transition of ChCl

	T_{ss}/K	$\Delta^{s\beta}_{s\alpha}H^\circ_m(T_{ss})$/ kJ mol^{-1}	$\Delta^{s\beta}_{s\alpha}S^\circ_m(T_{ss})$/ J K^{-1} mol^{-1}
This work	352.2 ± 0.6	16.3 ± 0.1	46.4 ± 0.8
Petrouleas and Lemmon[56]	351 ± 3	16.5 ± 0.2	47.0 ± 0.8

The expanded uncertainties of the experimental results, including the calibration uncertainty, were assigned based on independent experiments as $t \times s/\sqrt{n}$, where t is obtained from student's t-distribution (0.95 level of confidence), s is the standard deviation and n is the number of independent experiments.

The high precision heat capacity of ChCl at 298.15 K

The heat capacities at T = 298.15 K of choline chloride were measured using a high-precision heat capacity drop calorimeter, previously described in detail in the literature.[44–47] Details concerning the calibration and accuracy tests as well as the raw experimental data are provided in Section 3 of the ESI.† The stated accuracy of this methodology for the measurements of the heat capacities of liquids and solids at T = 298.15 K is better than 0.5%.

In Table 2, the standard molar heat capacities at 298.15 K of choline chloride are listed, together with the mass of sample, m_{sample}, used in two independent series of drop experiments, N_{drop}. The reported uncertainty is twice the standard deviation of the mean and includes the calibration uncertainty. The relative atomic masses used were those recommended by the IUPAC Commission in 2016,[58] the molar mass of choline chloride, M = 139.6242 g mol^{-1}.

The molar heat capacities of choline chloride have already been measured by Chemat *et al.*[59] using DSC in the temperature range from 303.15 K to 353.15 K. The derived molar heat capacity of choline chloride at T =298.15 K by Chemat *et al.*[59] (ChCl at 298.15 K = 191.9 J K^{-1} mol^{-1}) is significantly lower (10%) than the results present here. The magnitude of the deviation is attributed to the uncertainty of the results by Chemat *et al.*,[59] typical of heat capacity measurements performed by DSC.

The heat capacity temperature dependency of the solid choline chloride

The heat capacity of the α phase of choline chloride was measured by HC-DSC and the heat capacity of the β crystalline phase was measured by DSC. Both sets of data are listed in Table 3. The heat capacity for the α phase was additionally evaluated by DSC (experimental details, raw data and additional information are available in Section S4 in the ESI†). Fig. 5 depicts the molar heat capacities as a function of temperature for the α and β phases. The result obtained by drop calorimetry at 298.15 K of the α phase is also depicted. The experimental result derived by HC-DSC at 298.15 K (208.7 ± 1.0 J K^{-1} mol^{-1}) is in excellent agreement with that obtained by drop calorimetry (209.2 ± 0.8 J K^{-1} mol^{-1}). Considering the estimated uncertainty of the DSC measurements, the heat capacity results obtained for the α phase are in very good agreement with those obtained by

Table 2 Molar heat capacity $C^{\circ}_{p,m}$ results at T = 298.15 K for choline chloride. The calibration constant used to calculate $C^{\circ}_{p,m}$ was derived from sapphire [NBS, SRM 720, (α-Al_2O_3)] calibration (6.6541 ± 0.0206 W V^{-1})

Exp	m_{sample}/g	N_{drop}	$T_{furnace}$/K	$T_{calorimeter}$/K	T/K	$C^{\circ}_{p,m}$/J K^{-1} mol^{-1}	$C^{\circ}_{p,m}$/J K^{-1} mol^{-1}
I	0.36420	52	303.27	293.19	298.23	209.2 ± 0.8	209.2 ± 0.8
II	0.40293	11	303.25	293.20	298.22	209.5 ± 0.8	

N_{drop} = number of drop experiments; $T_{furnace}$ = average temperature of the furnace; $T_{calorimeter}$ = average temperature of the calorimeter; the uncertainty reported is twice the standard deviation of the mean and the calibration uncertainty is included.

Table 3 Experimental molar heat capacities of ChCl (α and β phases)

HC-DSC (α phase)		DSC (α phase)		DSC (β phase)	
T/K	$C^{\circ}_{p,m}$/J K^{-1} mol^{-1}	T/K	$C^{\circ}_{p,m}$/J K^{-1} mol^{-1}	T/K	$C^{\circ}_{p,m}$/J K^{-1} mol^{-1}
283.34	200.98	282.9	205.1	363.6	261.7
293.38	206.39	287.9	207.1	368.6	262.8
303.42	211.60	292.9	208.5	373.7	264.1
313.45	216.79	297.9	211.9	378.8	266.5
323.47	222.30	303.0	214.9	383.9	267.6
333.50	227.50	308.0	215.1	388.9	269.9
		322.9	219.3	394.0	272.0
		328.0	221.9	399.1	273.0
		333.0	224.1	404.2	274.4
		338.1	225.2	409.2	276.0
				414.3	278.0
				419.4	278.6

HC-DSC: heat-flow differential scanning microcalorimetry: $u(C^{\circ}_{p,m}) = 0.005$; $U(T)$ = 0.05 K. DSC: power compensation differential scanning calorimetry: $u(C^{\circ}_{p,m}) = 0.03$; $U(T)$ = 0.5 K.

HC-DSC, which supports the assigned uncertainty of the results obtained by DSC for the β crystalline phase of ChCl.

The experimental heat capacity data of the α and β phases of pure choline chloride were fitted with temperature, according to the following equation:

$$C^{\circ}_{p,m} = a + b \cdot (T/\mathrm{K}). \quad (1)$$

The a and b coefficients are listed in Table 4 for α and β phases considering the series of experimental results obtained in HC-DSC and in DSC, respectively.

The extrapolation of the heat capacity using the fitted equations was used to derive the heat capacity change of the α to β transition, $\Delta^{s\beta}_{s\alpha}C^{\circ}_{p,m}$, at the transition temperature (T_{ss} = 352.2 ± 0.6 K) as depicted in Fig. 5.

The calculated $\Delta^{s\beta}_{s\alpha}C^{\circ}_{p,m} = C^{\circ}_{p,m}(\beta, T_{ss}) - C^{\circ}_{p,m}(\alpha, T_{ss}) = 20 \pm 3$ J K^{-1} mol^{-1}, taken as the difference between the heat capacities of the α and β crystals at the solid–solid transition, is in excellent agreement with the estimated result (16 ± 5 J K^{-1} mol^{-1}) obtained in the study of the α to β transition of choline chloride by DSC. The temperature dependency coefficient "b" observed in the β phase (0.320 ± 0.007 J K^{-2} mol^{-1}) is significantly lower than the corresponding coefficient of the α phase (0.528 ± 0.003 J K^{-2} mol^{-1}), which is in agreement with the high entropy change observed in the α to β phase transition.

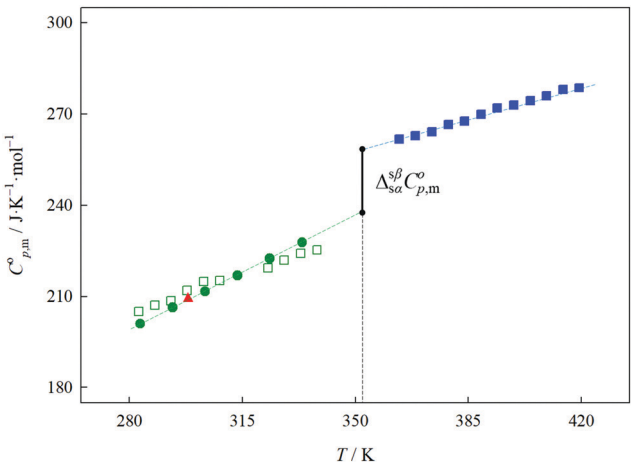

Fig. 5 Standard molar heat capacities, $C^{\circ}_{p,m}$, for the α and β crystalline phases of pure choline chloride. ●: α phase, HC-DSC; DSC [$(u(C^{\circ}_{p,m}) = 0.005$; $U(T)$ = 0.05 K)]; □: α phase, DSC [$u(C^{\circ}_{p,m}) = 0.03$; $U(T)$ = 0.5 K] ▲: α phase, Drop Cp; ■: β phase, DSC.

The estimation of the heat capacity of the hypothetical liquid ChCl

The heat capacities at T = 298.15 K of choline chloride and water binary mixtures (mole fraction $x_{ChCl} < 0.4$) were measured using a high-precision heat capacity drop calorimeter. The detailed experimental results and procedure are given in the ESI† (Section S3). Fig. 6 depicts the standard molar heat capacities of choline chloride and water binary mixtures, at T = 298.15 K, as a function of the mole fraction of choline chloride, x_{ChCl}. The hypothetical heat capacity of the liquid choline chloride at 298.15 K was estimated to be $C^{\circ}_{p,m}$ (ChCl, l, 298.15 K) = 249 ± 10 J K^{-1} mol^{-1} by the linear extrapolation of the heat capacities of

Table 4 The a and b coefficients of the molar heat capacity, $C^{\circ}_{p,m}$, of the pure crystalline phases of ChCl

Technique	Crystalline phase	T range/K	a/J K^{-1} mol^{-1}	b/J K^{-2} mol^{-1}	$\sigma_{r,fit}$ (%)
HC-DSC	α	283–333	51.3 ± 0.9	0.528 ± 0.003	0.2
DSC	β	363–419	145 ± 3	0.320 ± 0.007	0.4

$\sigma_{r,fit}(\%) = \sqrt{\frac{\sum_i^n \left(\frac{y - y_{fit}}{y_{fit}}\right)^2}{(n-m)}} \times 100$, in which n is the number of points used in the fit and m is the number of estimated parameters (in this case m = 2).

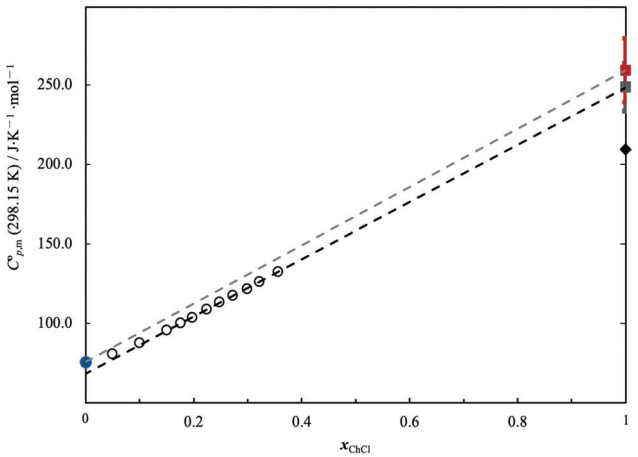

Fig. 6 Standard molar heat capacities [$(u(C^{\circ}_{p,m}) = 0.005$] at T = 298.15 K as a function of the molar fraction of choline chloride, x_{ChCl}, for choline chloride and water binary mixtures. ◆ ChCl (cr) and ■ ChCl (liq) (estimated), ● H_2O (liq), ○ mixtures of (ChCl + H_2O) with different compositions and ■ $C^{\circ}_{p,m}$(ChCl, liq) estimated by linear extrapolation.

the binary mixtures (ChCl + H_2O) in the molar fraction range of $0.2 < x_{ChCl} < 0.4$). The same result was compared with the estimated prediction of $C^{\circ}_{p,m}$(ChCl, liq, 298.15 K) = 259 ± 20 J K^{-1} mol^{-1}, obtained by the combination of the experimental result of the crystalline ChCl, $C^{\circ}_{p,m}$(ChCl, cr, 298.15 K) = 209.2 ± 0.8 J K^{-1} mol^{-1} and considering the typical solid–liquid heat capacity change of $\Delta^{l}_{cr}C^{\circ}_{p,m} \approx 50 \pm 20$ J K^{-1} mol^{-1}.[60,61] Both results are in good agreement.

Moreover, the analysis of the heat capacities of the binary mixtures indicates a negative excess heat capacity mixing in the region of the low mole fraction ChCl (0 to 0.2), followed by a quite linear relationship between 0.2 and 0.4 mole fractions of ChCl.

The solid–liquid phase diagram of choline chloride and water

The results of an extensive study of the solid–liquid equilibrium of the ChCl + water binary system obtained by DSC are presented in Fig. 7. The detailed information concerning the raw data for each mixture composition (mole fraction x_{ChCl}), eutectic temperatures, solid–solid transition temperatures, melting temperatures, and thermograms are available in the ESI† (Section S6).

The results reported in Fig. 7 show that the (ChCl + H_2O) system presents a eutectic type behavior (comparison to the literature in Fig. S7, ESI†) with a eutectic composition close to x_{ChCl} = 0.2 and a eutectic temperature of T = 204 K. It is remarkable that the solid–solid transition of the solid phase of choline chloride in the presence of water is observed at a temperature around 10 K below the temperature observed for the solid–solid transition in pure ChCl. This temperature shift should be related to the incorporation of water into the ChCl crystal structure observed by PXRD and discussed below.

The observed solid–solid transition, associated with the choline chloride, T_{ss} (ChCl) = 352.2 ± 0.6 K, presents an

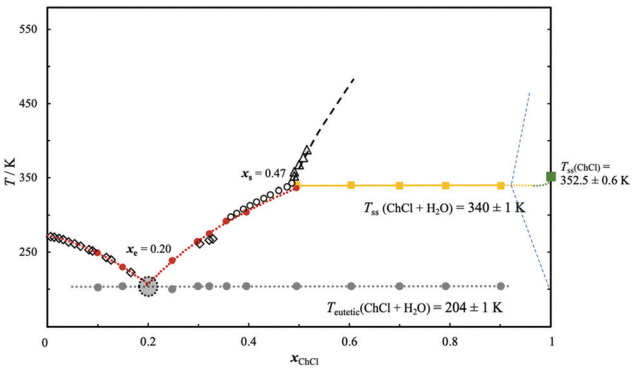

Fig. 7 Solid–liquid phase diagram (p = 0.10 ± 0.01 MPa) for the binary system choline chloride (ChCl) and water: ◇ – liquidus line (DSC NETZSCH); ○ – liquidus line (shake-flask);[35] △ – liquidus line (shake-flask); ● – liquidus line (DSC PerkinElmer); ■ – solid–solid transition of binary mixtures (ChCl + H_2O); ■ – solid–solid transition of ChCl; ● – eutectic transition. $U(T)$ = 1 K.

endothermic and reversible transition which was correlated with the mole fraction of ChCl as shown in the Tammann plot presented in Fig. 8. The intercept composition (based on the Tammann plot x_{ChCl} = 0.47) is in excellent agreement with the composition where the solid–liquid derivative discontinuity is observed in the correspondent phase diagram. However, its value does not extrapolate to the solid–solid enthalpy of the phase transition of pure ChCl. Instead, an estimated ΔH_{ss} = 17.3 ± 1.0 kJ mol^{-1} is obtained, which is 6% larger than that observed for pure ChCl. The differences observed in ΔH_{ss} and T_{ss} converge into the idea that the ChCl β solid phase is modified in the presence of water as discussed below.

Crystal structure resolution by PXRD

The hydrated sample of ChCl was studied at 358 K using powder X-ray diffraction revealing the presence of a poor crystalline material alongside with a significant amorphous component (see Fig. 9). The structure details were investigated using a long data acquisition which allowed the indexation of the powder pattern solely in the triclinic crystal system, mostly

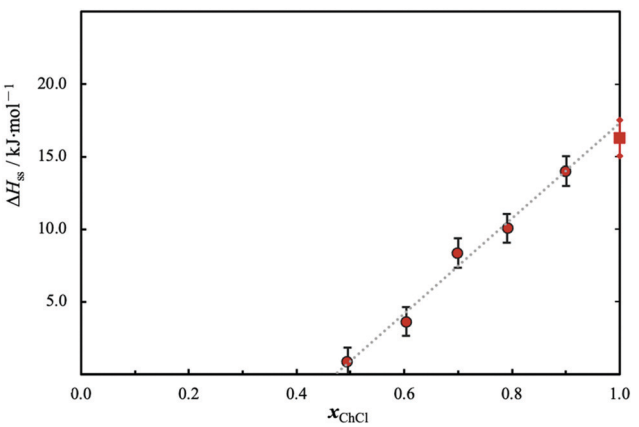

Fig. 8 Tammann diagram of the solid–solid transition for the binary system choline chloride and water. The solid–solid transition observed at T_{ss} = 340 ± 1 K. ■ ΔH_{ss} = 16.3 ± 0.1 kJ mol^{-1} (this work).

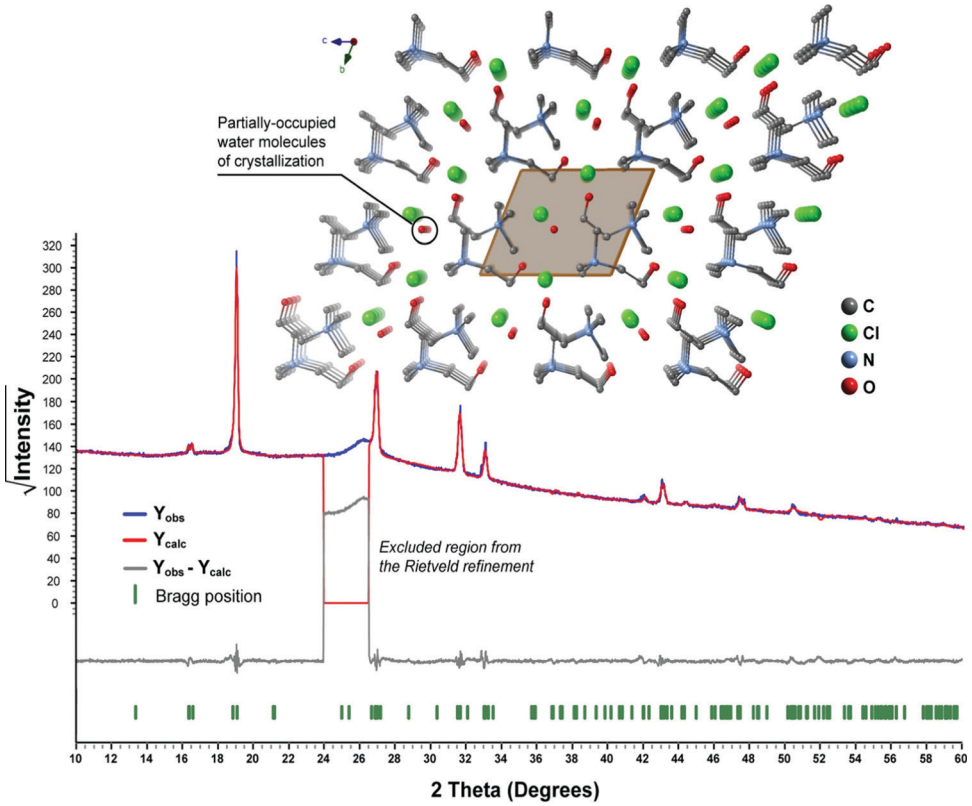

Fig. 9 Final Rietveld plot of ChCl treated at 358 K. The observed data points are indicated as a blue line, the best fit profile (upper trace) and the difference pattern (lower trace) are drawn as solid red and grey lines, respectively. Green vertical bars indicate the angular positions of the allowed Bragg reflections. Refinement details are given in Table S1 (ESI†). The inset depicts a perspective view along the [100] direction of the unit cell of the crystal structure model.

motivated by the poorly resolved and low-intensity few reflections available. A structure model could be derived only in *P*1 with the unit cell (see Table S1, ESI† for details; please note: unit cell not given as the Niggli reduced form) containing two chloride anions, two choline cations and a partially occupied water molecule of crystallization. Remarkably, this solution was reproducibly obtained starting from distinct molecular conformations, with the occupancy of the water molecule typically converging to a value around 0.20, which gives a 0.10 value per choline cation, *i.e.* a hydrated crystal with about $x_{ChCl} = 0.9$. The structure location of the water molecule (the inset in Fig. 9) permits the existence of supramolecular contacts (hydrogen bonds) with neighbouring chloride anions and the hydroxyl groups of the choline cation. This structural model fits well with the data acquired for the ChCl + H_2O solid–liquid phase diagram, indicating that the solid–solid transition occurs at a different temperature due to the inclusion of a small amount of water in the ChCl crystal structure, modifying it and creating a solid solution as suggested in the sketched phase diagram.

$^{13}C\{^1H\}$ CP MAS NMR studies (Fig. 10) on the starting material and that obtained by heating *in situ* up to 358 K corroborate the structural the aforementioned features: at ambient temperature, the material is poorly crystalline with the spectrum being dominated by a resonance centred at around 52.9 ppm; at 358 K, the material becomes overall more crystalline (structurally more organised), with the signal-to-noise clearly improving and with the observation of a broad resonance centred at around 70.5 ppm attributed to the –CH_2– moiety directly connected to the nitrogen of the choline cation. Noteworthy, the full width at half maximum of this resonance is larger than that attributed to the remaining resonances, in

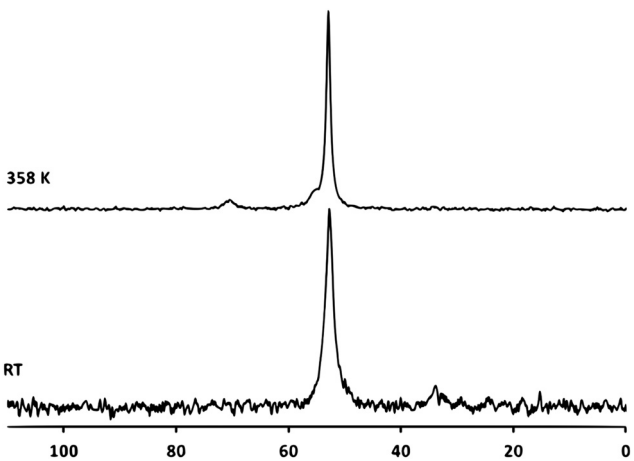

Fig. 10 $^{13}C\{^1H\}$ CP MAS NMR spectra of choline chloride collected at room temperature (RT) and after heating *in situ* up to 358 K.

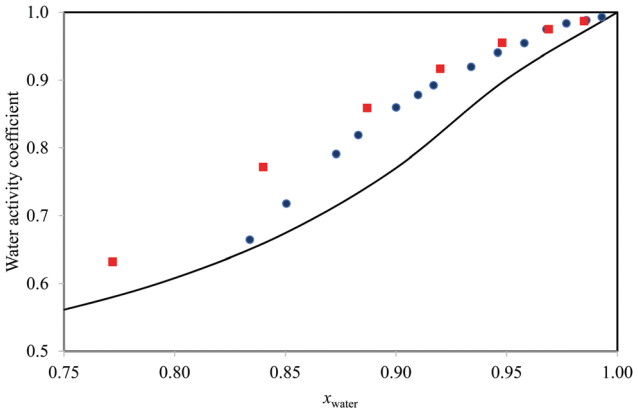

Fig. 11 Comparison of the water activity coefficients for the binary system ChCl + H_2O at different mole fractions (x_{water}) estimated from the SLE data measured in this work (●), estimated from the water activity data at 298.2 K (■) and COSMO-RS predictions at 298.2 K (solid black line).

agreement with the presence of two of such moieties in the *P*1 unit cell.

Thermodynamic assessment of the liquid phase non-ideality

The non-ideality of water in the studied system can be estimated from the melting point depression data as briefly described in the ESI† (Section S7). The resulting activity coefficients are presented in Fig. 11, where they are compared with the activity coefficients for water in the same system estimated from water activity measurements at 298.2 K.[62] The two sets of data are in good agreement, with the data estimated from the SLE measurements showing a slightly higher deviation from ideality due to being measured at lower temperatures, and the interactions between the two compounds, being dominated by hydrogen bonding and electrostatic contributions, are expected to increase as the temperature decreases. The COSMO-RS model[63–65] provides (for details, see Section S7, ESI†) a good description of the experimental data at 298.2 K, with some overestimation of the liquid phase non-ideality that is related to the lack of a term in COSMO-RS to describe the contribution of the long-range interactions. The COSMO-RS predictions are, nevertheless, reliable enough to be used to analyze the non-ideality of the liquid phase of this system.

The COSMO-RS predicted activity coefficients at 298.2 K for water and ChCl are shown in Fig. 12. In spite of the known tendency of the model to overestimate the non-ideality of this system, as discussed above, the model predictions show that for a ChCl composition range between mole fractions of 0.5 and 1, ChCl has a near-ideal behavior in the liquid phase. These small deviations from ideality are certainly further attenuated at the higher temperatures of this phase diagram. In this concentration range, there is very little dissociation of ChCl and the liquid phase is composed essentially of ion pairs.[33] This can explain the near-ideal behavior since, under these conditions, the molecular interactions are dominated by hydrogen bonding,[33,66] and no longer by electrostatic interactions, and water can supply broken hydrogen bonding resulting from the dissolution of ChCl.

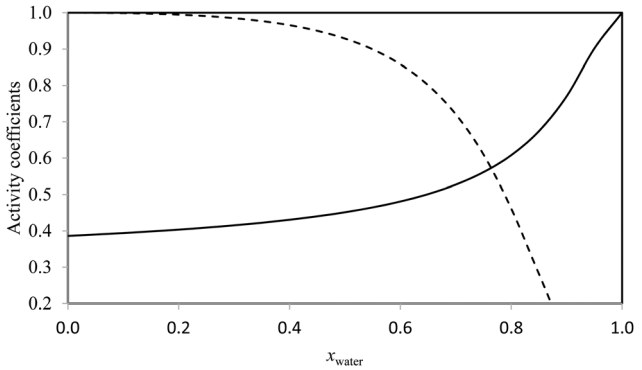

Fig. 12 COSMO-RS predicted activity coefficients at 298.2 K for water (solid line) and ChCl (dashed line) at different water mole fractions (x_{water}).

Conclusions

This work contributes significantly to increase knowledge on the characterization of ChCl and the solid–liquid phase diagram of the ChCl + H_2O binary system. The solid–solid (α to β) phase transition temperature (352.2 K) and enthalpy (16.3 kJ mol^{-1}) have been confirmed. Heat capacities of the α form have been measured between 283 and 333 K. For the β form, heat capacities are now known for the first time, in the temperature range between 363 and 419 K, allowing the estimation of heat capacity changes upon the solid–solid transition. Based on the data on the heat capacities of aqueous choline chloride solutions, it was possible to estimate the hypothetical heat capacity of the liquid (ChCl) of $\approx 249 \pm 10$ J K^{-1} mol^{-1} at 298.15 K.

Concerning the solid–liquid phase diagram, the eutectic point has been estimated to be at 204 K and the ChCl mole fraction close to 0.20. On the other hand, the solid–solid transition of the solid phase of choline chloride in the presence of water is observed at a temperature of around 10 K below the temperature observed for the solid–solid transition in pure ChCl. Therefore, a new structural model is proposed, including a small amount of water in the ChCl crystal structure, modifying it, and creating a solid solution that fits the SLE diagram and PXRD data. Finally, it was shown that water presents a strong negative deviation from ideality in the binary water + ChCl mixture while, when the solid phase is ChCl, choline chloride shows a behavior close to ideality.

Conflicts of interest

There are no conflicts to declare.

Acknowledgements

This work was supported by the Fundacão *para* a Ciência e Tecnologia (FCT) (funded by national funds through the FCT/MCTES (PIDDAC)) to CIQUP, the Faculty of Science, University of Porto (Project UIDB/00081/2020), the IMS-Institute of Molecular Sciences (LA/P/0056/2020), the CIMO-Mountain Research Center (Project UIDB/00690/2020), and the CICECO-Aveiro

Institute of Materials (Projects UIDB/50011/2020, UIDP/50011/2020 and LA/P/0006/2020). Support was also provided by project AllNat—POCI-01-0145-FEDER-030463 (PTDC/EQU-EPQ/30463/2017), funded by FEDER funds through COMPETE2020---Prog. Operacional Competitividade e Internacionalização (POCI), and by national funds through the Foundation for Science and Technology (FCT/MCTES). The NMR spectrometers are a part of the National NMR Network (PTNMR) and are partially supported by the Infrastructure Project No. 022161 (co-financed by FEDER through COMPETE 2020, POCI and PORL and FCT through PIDDAC). AIMCLF is also financed by national funds through the FCT-I.P., in the framework of the execution of the program contract provided in paragraphs 4, 5 and 6 of art. 23 of Law no. 57/2016 of 29 August, as amended by Law no. 57/2017 of 19 July. Sérgio M. Vilas-Boas acknowledges the FCT and European Social Fund (ESF) for his PhD grant (SFRH/BD/138149/2018).

References

1 F. Ullmann and M. Bohnet, *Ullmann's encyclopedia of industrial chemistry*, Wiley-VCH, 7th edn, 2009.
2 A. P. Abbott, G. Capper, D. L. Davies, R. K. Rasheed and V. Tambyrajah, Novel solvent properties of choline chloride urea mixtures, *Chem. Commun.*, 2003, 70–71.
3 A. P. Abbott, D. Boothby, G. Capper, D. L. Davies and R. Rasheed, Deep Eutectic Solvents Formed Between Choline Chloride and Carboxylic Acids, *J. Am. Chem. Soc.*, 2004, **126**, 9142.
4 Z. Maugeri and P. Domínguez De María, Novel choline-chloride-based deep-eutectic-solvents with renewable hydrogen bond donors: Levulinic acid and sugar-based polyols, *RSC Adv.*, 2012, **2**, 421–425.
5 I. M. Aroso, A. Paiva, R. L. Reis and A. R. C. Duarte, Natural deep eutectic solvents from choline chloride and betaine – Physicochemical properties, *J. Mol. Liq.*, 2017, **241**, 654–661.
6 C. Ruß and B. König, Low melting mixtures in organic synthesis - An alternative to ionic liquids?, *Green Chem.*, 2012, **14**, 2969–2982.
7 Y. Dai, G. J. Witkamp, R. Verpoorte and Y. H. Choi, Tailoring properties of natural deep eutectic solvents with water to facilitate their applications, *Food Chem.*, 2015, **187**, 14–19.
8 D. O. Abranches, L. P. Silva, M. A. R. Martins, L. Fernandez, S. P. Pinho and J. A. P. Coutinho, Can cholinium chloride form eutectic solvents with organic chloride-based salts?, *Fluid Phase Equilib.*, 2019, **493**, 120–126.
9 E. L. Smith, A. P. Abbott and K. S. Ryder, Deep Eutectic Solvents (DESs) and Their Applications, *Chem. Rev.*, 2014, **114**, 11060–11082.
10 Y. Zhang, X. Ji and X. Lu, Choline-based deep eutectic solvents for CO2 separation: Review and thermodynamic analysis, *Renewable Sustainable Energy Rev.*, 2018, **97**, 436–455.
11 A. Abo-Hamad, M. Hayyan, M. A. AlSaadi and M. A. Hashim, Potential applications of deep eutectic solvents in nanotechnology, *Chem. Eng. J.*, 2015, **273**, 551–567.
12 L. I. N. Tomé, V. Baião, W. da Silva and C. M. A. Brett, Deep eutectic solvents for the production and application of new materials, *Appl. Mater. Today*, 2018, **10**, 30–50.
13 A. Roda, A. A. Matias, A. Paiva and A. R. C. Duarte, Polymer science and engineering using deep eutectic solvents, *Polymers*, 2019, **11**, 1–22.
14 J. Huang, X. Guo, T. Xu, L. Fan, X. Zhou and S. Wu, Ionic deep eutectic solvents for the extraction and separation of natural products, *J. Chromatogr. A*, 2019, **1598**, 1–19.
15 L. Fernandez, L. P. Silva, M. A. R. Martins, O. Ferreira, J. Ortega, S. P. Pinho and J. A. P. Coutinho, Indirect assessment of the fusion properties of choline chloride from solid–liquid equilibria data, *Fluid Phase Equilib.*, 2017, **448**, 9–14.
16 Q. Zhang, K. De Oliveira Vigier, S. Royer and F. Jérôme, Deep eutectic solvents: Syntheses, properties and applications, *Chem. Soc. Rev.*, 2012, **41**, 7108–7146.
17 D. Carriazo, M. C. Serrano, M. C. Gutiérrez, M. L. Ferrer and F. del Monte, Deep-eutectic solvents playing multiple roles in the synthesis of polymers and related materials, *Chem. Soc. Rev.*, 2012, **41**, 4996–5014.
18 M. A. R. Martins, S. P. Pinho and J. A. P. Coutinho, Insights into the nature of eutectic and deep eutectic mixtures, *J. Solution Chem.*, 2019, **48**, 962–982.
19 Y. Marcus, *Deep Eutectic Solvents*, Springer International Publishing, Cham, 2019, pp. 111–151.
20 M. Vilková, J. Płotka-Wasylka and V. Andruch, The role of water in deep eutectic solvent-base extraction, *J. Mol. Liq.*, 2020, **304**, 112747.
21 T. El Achkar, S. Fourmentin and H. Greige-gerges, Deep eutectic solvents: An overview on their interactions with water and biochemical compounds, *J. Mol. Liq.*, 2019, **288**, 111028.
22 R. Alcalde, A. Gutiérrez, M. Atilhan and S. Aparicio, An experimental and theoretical investigation of the physicochemical properties on choline chloride – Lactic acid based natural deep eutectic solvent (NADES), *J. Mol. Liq.*, 2019, **290**, 110916.
23 D. O. Abranches, L. P. Silva, M. A. R. Martins and J. A. P. Coutinho, Differences on the impact of water on the deep eutectic solvents betaine/urea and choline/urea, *J. Chem. Phys.*, 2021, **155**, 034501.
24 L. Sapir and D. Harries, Restructuring a deep eutectic solvent by water: The nanostructure of hydrated choline chloride/urea, *J. Chem. Theory Comput.*, 2020, **16**, 3335–3342.
25 F. Gabriele, M. Chiarini, R. Germani, M. Tiecco and N. Spreti, Effect of water addition on choline chloride/glycol deep eutectic solvents: Characterization of their structural and physicochemical properties, *J. Mol. Liq.*, 2019, **291**, 111301.
26 T. Zhekenov, N. Toksanbayev, Z. Kazakbayeva, D. Shah and F. S. Mjalli, Formation of type III Deep Eutectic Solvents and effect of water on their intermolecular interactions, *Fluid Phase Equilib.*, 2017, **441**, 43–48.
27 N. López-Salas, J. M. Vicent-Luna, S. Imberti, E. Posada, M. J. Roldán, J. A. Anta, S. R. G. Balestra, R. M. Madero

Castro, S. Calero, R. J. Jiménez-Riobóo, M. C. Gutiérrez, M. L. Ferrer and F. Del Monte, Looking at the 'water-in-Deep-Eutectic-Solvent' System: A Dilution Range for High Performance Eutectics, *ACS Sustainable Chem. Eng.*, 2019, **7**, 17565–17573.

28 V. Alizadeh, F. Malberg, A. A. H. Pádua and B. Kirchner, Are there magic compositions in deep eutectic solvents? Effects of composition and water content in choline chloride/ethylene glycol from ab initio molecular dynamics, *J. Phys. Chem. B*, 2020, **124**, 7433–7443.

29 S. Rozas, C. Benito, R. Alcalde, M. Atilhan and S. Aparicio, Insights on the water effect on deep eutectic solvents properties and structuring: The archetypical case of choline chloride + ethylene glycol, *J. Mol. Liq.*, 2021, **344**, 117717.

30 Y. Rublova, A. Kityk, F. Danilov and V. Protsenko, Mechanistic study on surface tension of binary and ternary mixtures containing choline chloride, ethylene glycol and water (components of aqueous solutions of a deep eutectic solvent, Ethaline), *Z. Phys. Chem.*, 2020, **234**, 399–413.

31 D. Lapeña, L. Lomba, M. Artal, C. Lafuente and B. Giner, Thermophysical characterization of the deep eutectic solvent choline chloride:ethylene glycol and one of its mixtures with water, *Fluid Phase Equilib.*, 2019, **492**, 1–9.

32 H. Zhang, M. L. Ferrer, M. J. Roldán-Ruiz, R. J. Jiménez-Riobóo, M. C. Gutiérrez and F. Del Monte, Brillouin Spectroscopy as a suitable technique for the determination of the eutectic composition in mixtures of choline chloride and water, *J. Phys. Chem. B*, 2020, **124**, 4002–4009.

33 A. Triolo, F. Lo Celso, M. Brehm, V. Di Lisio and O. Russina, Liquid structure of a choline chloride–water natural deep eutectic solvent: A molecular dynamics characterization, *J. Mol. Liq.*, 2021, **331**, 115750.

34 M. S. Rahman and D. E. Raynie, Thermal behavior, solvatochromic parameters, and metal halide solvation of the novel water-based deep eutectic solvents, *J. Mol. Liq.*, 2021, **324**, 114779.

35 S. M. Vilas-boas, D. O. Abranches, E. A. Crespo, O. Ferreira, J. A. P. Coutinho and S. P. Pinho, Experimental solubility and density studies on aqueous solutions of quaternary ammonium halides, and thermodynamic modelling for melting enthalpy estimations, *J. Mol. Liq.*, 2020, **300**, 112281.

36 A. Coelho, *Topas Academic, Version 5.0, Coelho Software*, Brisbane, 2013.

37 A. A. Coelho, Indexing of powder diffraction patterns by iterative use of singular value decomposition, *J. Appl. Crystallogr.*, 2003, **36**, 86–95.

38 H. M. Rietveld, A profile refinement method for nuclear and magnetic structures, *J. Appl. Crystallogr.*, 1969, **2**, 65–71.

39 R. W. Cheary and A. Coelho, A fundamental parameters approach to X-ray line-profile fitting, *J. Appl. Crystallogr.*, 1992, **25**, 109–121.

40 R. Sabbah, A. Xu-wu, J. S. Chickos, M. L. P. Leitão, M. V. Roux and L. A. Torres, Reference materials for calorimetry and differential thermal analysis, *Thermochim. Acta*, 1999, **331**, 93–204.

41 G. Blanquart and H. Pitsch, Thermochemical properties of polycyclic aromatic hydrocarbons (PAH) from G3MP2B3 calculations, *J. Phys. Chem. A*, 2007, **111**, 6510–6520.

42 G. Della Gatta, M. J. Richardson, S. M. Sarge and S. Stølen, Standards, calibration, and guidelines in microcalorimetry. Part 2. Calibration for differential scanning calorimetry (IUPAC Technical Report), *Pure Appl. Chem.*, 2006, **78**, 1455–1476.

43 E. S. Domalski and E. D. Hearing, Heat capacities and entropies of organic compounds in the condensed phase. Volume III, *J. Phys. Chem. Ref. Data*, 1996, **25**, 1–525.

44 J. S. Konicek, J. Suurkuusk and I. Wadsö, A precise drop heat capacity calorimeter for small samples, *Chem. Scr.*, 1971, **1**, 217–220.

45 J. Suurkuusk and I. Wadsö, Design and testing of an improved precise drop calorimeter for the measurement of the heat capacity of small samples, *J. Chem. Thermodyn.*, 1974, **6**, 667–679.

46 L. M. N. B. F. Santos, M. A. A. Rocha, A. S. M. C. Rodrigues, V. Štejfa, M. Fulem and M. Bastos, Reassembling and testing of a high-precision heat capacity drop calorimeter. Heat capacity of some polyphenyls at T = 298.15 K, *J. Chem. Thermodyn.*, 2011, **43**, 1818–1823.

47 C. E. S. Bernardes, L. M. N. B. F. Santos and M. E. M. Da Piedade, A new calorimetric system to measure heat capacities of solids by the drop method, *Meas. Sci. Technol.*, 2006, **17**, 1405–1408.

48 D. A. Ditmars, S. Ishihara, S. S. Chang, G. Bernstein and E. D. West, Enthalpy and heat-capacity standard reference material: Synthetic sapphire (alpha-Al2O3) from 10 to 2250 K, *J. Res. Natl. Bur. Stand. (1934).*, 1982, **87**, 159.

49 T. Kousksou, A. Jamil, Y. Zeraouli and J. P. Dumas, DSC study and computer modelling of the melting process in ice slurry, *Thermochim. Acta*, 2006, **448**, 123–129.

50 T. Kousksou, A. Jamil, Y. Zeraouli and J. P. Dumas, Equilibrium liquidus temperatures of binary mixtures from differential scanning calorimetry, *Chem. Eng. Sci.*, 2007, **62**, 6516–6523.

51 A. Jamil, T. Kousksou, Y. Zeraouli and J. P. Dumas, Liquidus temperatures determination of the dispersed binary system, *Thermochim. Acta*, 2008, **471**, 1–6.

52 S. Noshadi and R. Sadeghi, Differential scanning calorimetry determination of phase diagrams and water activities of aqueous carboxylic acid solutions, *Thermochim. Acta*, 2018, **663**, 46–52.

53 S. Noshadi and R. Sadeghi, Differential scanning calorimetry determination of Solid−Liquid equilibria phase diagrams for binary monocarboxylic acids solutions, *Fluid Phase Equilib.*, 2019, **486**, 1–10.

54 S. M. Vilas-Boas, P. Brandão, M. A. R. Martins, L. P. Silva, T. B. Schreiner, L. Fernandes, O. Ferreira and S. P. Pinho, Solubility and solid phase studies of isomeric phenolic acids in pure solvents, *J. Mol. Liq.*, 2018, **272**, 1048–1057.

55 S. M. Vilas-Boas, R. S. Alves, P. Brandão, L. M. A. Campos, J. A. P. Coutinho, S. P. Pinho and O. Ferreira, Solid–liquid phase equilibrium of trans-cinnamic acid, p-coumaric acid

and ferulic acid in water and organic solvents: Experimental and modelling studies, *Fluid Phase Equilib.*, 2020, **521**, 112747.

56 V. Petrouleas and R. M. Lemmon, Calorimetric studies of choline chloride, bromide, and iodide, *J. Chem. Phys.*, 1978, **69**, 1315–1316.

57 P. B. P. Serra, F. M. S. Ribeiro, M. A. A. Rocha, M. Fulem, K. Růžička, J. A. P. Coutinho and L. M. N. B. F. Santos, Solid–liquid equilibrium and heat capacity trend in the alkylimidazolium PF6 series, *J. Mol. Liq.*, 2017, **248**, 678–687.

58 M. E. Wieser, N. Holden, T. B. Coplen, J. K. Böhlke, M. Berglund, W. A. Brand, P. De Bièvre, M. Gröning, R. D. Loss, J. Meija, T. Hirata, T. Prohaska, R. Schoenberg, G. O'Connor, T. Walczyk, S. Yoneda and X.-K. Zhu, Atomic weights of the elements 2011 (IUPAC Technical Report), *Pure Appl. Chem.*, 2013, **85**, 1047–1078.

59 F. Chemat, H. Anjum, A. M. Shariff, P. Kumar and T. Murugesan, Thermal and physical properties of (choline chloride + urea + l-arginine) deep eutectic solvents, *J. Mol. Liq.*, 2016, **218**, 301–308.

60 J. S. Chickos, A protocol for correcting experimental fusion enthalpies to 298.15 K and it's application in indirect measurements of sublimation enthalpy at 298.15 K, *Thermochim. Acta*, 1998, **313**, 19–26.

61 N. V. Sidgwick, *Strengths of Chemical Bonds*, Butterworths, London, 1954, p. 104.

62 I. Khan, K. A. Kurnia, T. E. Sintra, J. A. Saraiva, S. P. Pinho and J. A. P. Coutinho, Assessing the activity coefficients of water in cholinium-based ionic liquids: Experimental measurements and COSMO-RS modeling, *Fluid Phase Equilib.*, 2014, **361**, 16–22.

63 A. Klamt, Conductor-like screening model for real solvents: A new approach to the quantitative calculation of solvation phenomena, *J. Phys. Chem.*, 1995, **99**, 2224–2235.

64 A. Klamt, V. Jonas, T. Bürger and J. C. W. Lohrenz, Refinement and parametrization of COSMO-RS, *J. Phys. Chem. A*, 1998, **102**, 5074–5085.

65 A. Klamt and F. Eckert, COSMO-RS: a novel and efficient method for the a priori prediction of thermophysical data of liquids, *Fluid Phase Equilib.*, 2000, **172**, 43–72.

66 K. M. Harmon, A. C. Akin, G. F. Avci, L. S. Nowos and M. B. Tierney, Hydrogen bonding. Part 33. NMR study of the hydration of choline and acetylcholine halides, *J. Mol. Struct.*, 1991, **244**, 223–236.